JACS
JOURNAL OF THE AMERICAN CHEMICAL SOCIETY
Article
pubs.acs.org/JACS

Manipulating the Interfacial Energetics of n-type Silicon Photoanode for Efficient Water Oxidation

Tingting Yao,[†,‡] Ruotian Chen,[†,‡,∥] Junjie Li,[⊥] Jingfeng Han,[†,‡,§] Wei Qin,[†,‡] Hong Wang,[†,‡,∥] Jingying Shi,[†,‡] Fengtao Fan,[†,‡,§] and Can Li*[,†,‡,§]

[†]State Key Laboratory of Catalysis, [‡]Dalian National Laboratory for Clean Energy, [§]The Collaborative Innovation Center of Chemistry for Energy Materials (iChEM), Dalian Institute of Chemical Physics, Chinese Academy of Sciences, Zhongshan Road 457, Dalian 116023, China

[∥]University of Chinese Academy of Sciences, Beijing 100049, China

[⊥]International Iberian Nanotechnology Laboratory (INL), Avenida Mestre Jose Veiga, Braga 4715-330, Portugal

Supporting Information

ABSTRACT: The photoanodes with heterojunction behavior could enable the development of solar energy conversion, but their performance largely suffers from the poor charge separation and transport process through the multiple interfacial energy levels involved. The question is how to efficiently manipulate these energy levels. Taking the n-Si Schottky photoanode as a prototype, the undesired donor-like interfacial defects and its adverse effects on charge transfer in n-Si/ITO photoanode are well recognized and diminished through the treatment on electronic energy level. The obtained n-Si/TiO_x/ITO Schottky junction exhibits a highly efficient charge transport and a barrier height of 0.95 eV, which is close to the theoretical optimum for n-Si/ITO Schottky contact. Then, the holes extraction can be further facilitated through the variation of surface energy level, with the NiOOH coated ITO layer. This is confirmed by a 115% increase in surface photovoltage of the photoanodes. Eventually, an unprecedentedly low onset potential of 0.9 V (vs RHE) is realized for water oxidation among n-Si photoanodes. For the water oxidation reaction, the n-Si/TiO_x/ITO/NiOOH photoanode presents a charge separation efficiency up to 100% and an injection efficiency greater than 90% at a wide voltage range. This work identifies the important role of interfacial energetics played in photoelectrochemical conversion.

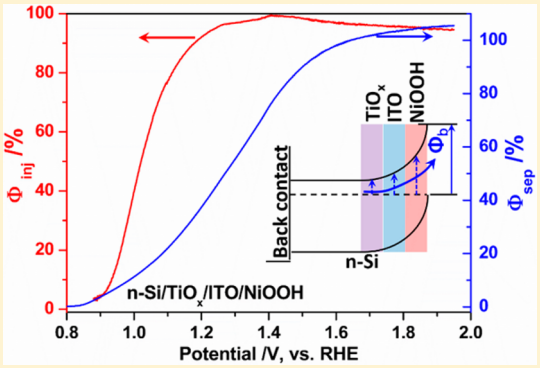

1. INTRODUCTION

Photoelectrochemical (PEC) water splitting has been recognized as a highly desirable approach to convert solar energy into storable fuels. The photoinduced charge is generated in a semiconductor photoelectrode and needs to be separated efficiently in the space charge region (SCR) in order to participate in the photoelectrolytic reactions.[1] The built-in electric field, whose intensity is closely related to the barrier height of the junction in the photoelectrode, largely determines the efficiency of photoinduced charge separation and transport.[2] So, the fundamental problem is how to enlarge the barrier height of the junction in a photoelectrode. According to the Schottky−Mott rule, the Schottky barrier height should be closely associated with the work function of the metal relative to the electron affinity of silicon in a n-Si Schottky photoanode.[3,4] But in practice, when n-Si is attached to the metal, the overlapped wave functions will lead to the charge redistribution and bond rearrangement at the interface. The rearranged chemical bonding has a large impact on the interfacial energetics, and then alters the barrier height of the junction.[5,6]

As the charge transfer only takes place over several atomic planes at the interface, the photovoltaic behavior of Schottky photoanodes sensitively varies under the influence of interfacial energetics. Taking Si/ITO (indium doped tin dioxide, ITO) contact as an example, nowadays, the ITO was usually used to passivate the Si photoanodes with buried np^+ homojunction and form an ohmic contact with the silicon substrate. The ITO merely acted as the protection layer and the photovoltage was mainly generated from the np^+ homojunction.[7−10] Directly depositing the ITO on n-Si caused a reduced onset potential and increased overpotential for a certain current density, because of the poor photovoltage generated from the n-Si/ITO Schottky junctions compared with that from the np^+-Si homojunction.[11] The poor photovoltage indicates a bad n-Si/ITO contact and a lower barrier height. Ashok and Wiley have demonstrated an extreme case that an ohmic contact could be formed between ITO and n-Si through an ion-beam treated interface.[12] Considering the transparent property and high

Received: July 16, 2016
Published: September 22, 2016

DOI: 10.1021/jacs.6b07188
J. Am. Chem. Soc. 2016, 138, 13664−13672

work function of the ITO, a diminished light-blocking and large barrier height can be expected for n-Si/ITO Schottky photoanodes.[13−15] But until now, there was no report for such kind of photoanodes with appreciable PEC behavior. So, it is worthwhile to understand the affinity between the barrier height and the energetics at the n-Si/ITO interface, in order to optimize the photovoltaic behavior of the photoanodes.

Layered nickel oxide hydroxide (NiOOH) have attracted a widespread attention due to its unique structure and good OER activity in alkaline medium.[16,17] Its OER activity can be adjusted according to the film thickness.[18,19] Coupling NiOOH on photoanodes can effectively suppress the electron−hole pair recombination and accelerate reaction kinetics at the photoelectrode/electrolyte interface.[20,21] A transition between NiO/$Ni(OH)_2$ to NiO/NiOOH exists in the film during water oxidation in alkali solution.[22] The redox potential of α-$Ni(OH)_2$/γ-NiOOH is smaller than that of β-$Ni(OH)_2$/β-NiOOH due to the larger intersheet distance and charge capacity of the former transition than latter.[23] Beyond this, by varying the amount of dopants (Fe, Co), the doped nickel oxide hydroxide behaves various OER activities and redox potential, which might be critical for coupling with a photoanode of proper energy band alignment.[24−26] Here, the undoped NiOOH with a low redox potential will be deposited for coupling with n-Si photoanode through electro-oxidation deposition method.

Herein, we will present a set of analysis on the relationship between interface energy levels and the charge transport, aiming to illustrate the impact of interface states on the PEC behavior of the n-Si/ITO Schottky photoanodes. The midgap electronic states of the material and chemical bonding are also investigated in details, thereby offering an approach to optimizing the performance of the photoanodes. Moreover, the promotion role of the surface contacted oxygen evolution catalyst (OEC) in enhancing the charge separation is also proved through the surface photovoltage (SPV) measurement on the photoanodes. Eventually, an n-Si/TiO_x/ITO/NiOOH photoanode with high water oxidation performance will be achieved. This study demonstrates the feasibility of such an interfacial engineering strategy to enhance the PEC performance of a Schottky photoanode.

2. ENERGETICS CALCULATION

The effective density of states in the conduction band of silicon was calculated following the equation

$$N_C = 2\left(\frac{2\pi m_e^* kT}{h^2}\right)^{3/2}$$

where h is the Planck constant (6.626×10^{-34} J s), m_e^* is the electron effective mass of silicon ($1.09m_e$ at 300 K, $m_e = 9.109 \times 10^{-31}$ kg is the electron rest mass), κ is the Boltzmann constant (1.38×10^{-23} J K^{-1}), and temperature is T (300 K). Then, the calculated N_C value is 2.85×10^{25} m^{-3}.

The gap in energy between the Fermi level and the conduction band of n-Si could be calculated by using the equation as follows

$$V_n = \frac{\kappa T}{q} \ln(N_C/N_D)$$

The donor density (N_D) of the silicon wafer (100) was measured using a four-point probe method, and calculated from the equation, $N_D = 1/q\mu\rho$, where q is the charge of an electron (1.6×10^{-19}), μ is the electron mobility (531 cm^2 V^{-1} s^{-1}), and ρ is the resistivity (0.3394 ohm cm). Then, the n-Si wafer has a donor density of 3.5×10^{16} cm^{-3}. The density of states in the conduction band (N_C) was calculated in the previous paragraph (2.8×10^{19} cm^{-3}), κ is the Boltzmann's constant (1.38×10^{-23} J K^{-1}) and temperature is T (298 K).[27] V_n is calculated to be 0.17 eV.

3. RESULTS AND DISCUSSION

3.1. Role of Interfacial States on PEC Behavior of Photoanodes. *3.1.1. The Impact of the Donor-like Interfacial Defects.* ITO is a degenerate semiconductor with high conductivity, acting more like a metal than as a semiconductor. We fabricated the n-Si/ITO photoelectrode, and checked its photoelectronic transport property using a reversible redox couples $Fe(CN)_6^{3-/4-}$ (Figures 1 and S1).[14]

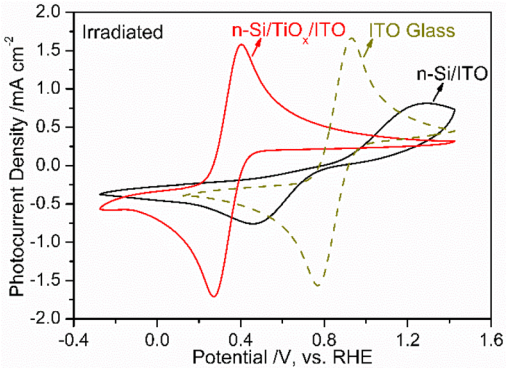

Figure 1. . Cyclic voltammetry (CV) curves of the n-Si/ITO and n-Si/TiO_x/ITO photoelectrodes tested in 5 mM ferri/ferrocyanide solution under 100 mW cm^{-2} of simulated AM1.5 G solar illumination. The CV curve of the nonphotoactive ITO glass is also shown, indicating the apparent redox potential of the Fe (II/III) electrolyte under the testing condition.

Compared with the result obtained with the ITO glass in the dark, the n-Si/ITO photoelectrode shows a more positive Fe (II) oxidation potential even being irradiated, indicating that the holes hardly arrive at the electrode surface and participate in the Fe(II) oxidation reaction. This is deviated from the theoretical expectation, which proposes a facile outward transport for photoinduced holes in n-type semiconductor (Figure S2).

We used an ITO layer of 50 nm thickness in n-Si/ITO for solid-state device measurement (Figure S4), where forward bias was defined as a positive pole of DC voltage applied on the ITO gate electrode. As shown in Figure 2, the current−voltage curves of the n-Si/ITO solid cell present a certain rectifying effect in the dark. The thermally emitted electron current is largely enhanced under applied positive potential, suggesting an upward band bending existed in the depletion region of n-Si. But the n-Si/ITO Schottky cell can only give a negligible open circuit voltage (V_{oc}, 60 mV) under illumination. This extremely low V_{oc} even could not afford the overpotential needed for charge tunneling through the electric double layer in solution, resulting in a more positive Fe(II) oxidation potential than ITO glass.

The capacitance−voltage profiling was used to explore some properties near the silicon surface, such as the built-in electric field, interface charge or states, inversion behavior and so on. As

DOI: 10.1021/jacs.6b07188
J. Am. Chem. Soc. 2016, 138, 13664−13672

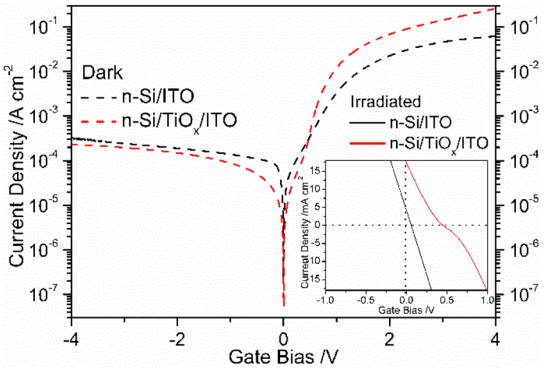

Figure 2. Current−voltage curves of the n-Si/ITO and n-Si/TiO$_x$/ITO solid-state cells in the dark (dash lines). The inset shows the photovoltaic responses of the same devices under illumination (solid lines).

illustrated in Figure 3, the capacitance−voltage curves were measured under a sufficiently low frequency (100 Hz) to get

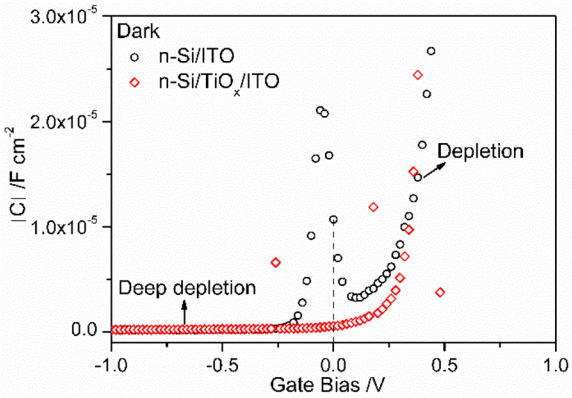

Figure 3. Capacitance−voltage curves recorded for n-Si/ITO and n-Si/TiO$_x$/ITO solid cells with 100 Hz AC frequency in the dark.

more information involved. As for the n-Si/ITO Schottky cell, the SCR near the silicon surface has been depleted since the gate bias is lower than 0.5 V, but the depletion region could not be directly transitioning into the deep depletion region under reverse bias, with the appearance of an incremental capacitance between the depletion and deep depletion regions.[28] The appeared capacitance peak suggests the existence of some ionized species, which contribute to the charge change ($d\rho/dV$) in the Schottky junction.[29]

Scheme 1 simulates the energy band diagram and the SCR of the n-Si/ITO Schottky device in the presence of a donor-like deep defects. For simplicity, it is assumed that the defect levels are discrete.[30] When the donor-like deep defects are all located below the Fermi energy level and filled with electrons, they present charge neutral and have no contributions for the total capacitance. With increasing the reverse bias, the donor-like deep defects level are moved up, along with the moved energy band, and eventually moved above the Fermi level. Then, the deep defects are ionized and have positive charge. The measured capacitance can be characterized as the combination of the capacitances corresponding to the SCR and the ionized defects.

Based on the illustration in Scheme 1, there must be some donor-like defects existed in the n-Si/ITO Schottky device, and these donor-like states are partially ionized under equilibrium

Scheme 1. Energy Band Diagram of the n-Si/ITO Schottky Device Where the n-Si Contains a Donor-like Species, and the Change of Charge Density Induced by the Incremental Change of Reverse Bias

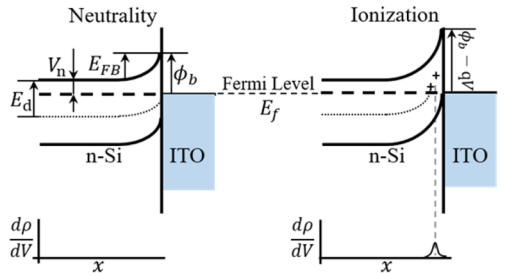

states, which behaved as an enhanced capacitance at 0 V gate bias. More donor-like states are ionized with applied reverse bias, resulting in a further increased capacitance. With increasing the reverse bias, when the donor-like energy levels pass through the Fermi level at the n-Si surface, the percentage changes in capacitance attains the maximum value. Then, the defect energy level can be directly calculated according to the relationship as follows.[31]

$$E_d - E_{CB} = \Phi_b - qV$$

Here, the barrier height (Φ_b) minus the energy band shift (qV), which is related to the applied voltage corresponding to the minima in Figure 4, is equal to the donor-like defect energy

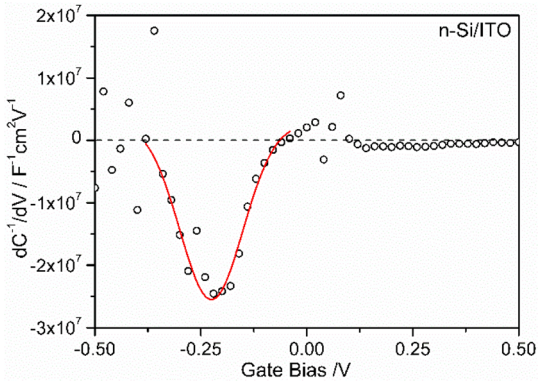

Figure 4. Derivative of the nonlinear capacitance−voltage curve for the donor-like defects of n-Si/ITO cell in Figure 3, and its fit with Gaussian line shape.

level (E_d) relative to the conduction band edge (E_{CB}) in the n-Si. The barrier height (Φ_b = 0.62 eV) can be calculated from the flat band potential (E_{FB}, Figure S5a) and the gap (V_n) between the Fermi level and the conduction band of n-Si. The voltage (V), where the $\left(\frac{dC^{-1}}{dV}\right)$ vs bias relationship reaches the minima, is about −0.22 V. Then, the donor-like defects are located at 0.84 eV below the conduction band of n-Si ($E_{CB,Si}$).

3.1.2. Enhanced Performance through Interfacial Modification. At the Si/SiO$_x$ interface, the silicon atoms are always have unsaturated dangling bonds, which will result in a high density of interface states. These interface defects are electrically active and act as the donor-like or acceptor-like energy levels in the Si band gap.[32] To weaken the undesirable electrically activities from the interface states, a thin layer of TiO$_x$ was introduced to modify the interfacial contact. As

DOI: 10.1021/jacs.6b07188
J. Am. Chem. Soc. 2016, 138, 13664−13672

shown in the CV curves (Figure 1), an obvious oxidation peak for Fe(II) can be observed for the irradiated n-Si/TiO_x/ITO photoanode. Here, the potential needed for Fe(II) photooxidation is more negative compared with the apparent oxidation potential obtained with ITO glass, suggesting that the photoinduced holes of n-Si are readily involved in the surface oxidation reaction.[33] At the same time, the Fe(III) reduction reaction takes place at more negative potential after imposing the illumination, implying a light induced blocking for electrons. The enhanced photocurrent density of the n-Si/TiO_x/ITO photoanode indicates the increased usable charges which may be attributed to a suppressed charge recombination after the modification with TiO_x. From the current−voltage curve of the n-Si/TiO_x/ITO solid-state cell (Figure 2), it can be observed that the reverse saturation current of the n-Si/TiO_x/ITO is suppressed compared to that of n-Si/ITO in the dark, together with the largely enhanced forward output current, demonstrating a higher rectification ratio and a lower leakage for Si/TiO_x/ITO device. The lower leakage current suggests the suppression of the charge recombination after using the TiO_x interlayer.[34] Under illumination, a positive current was detected under no biased condition (Figure 2, inset). It means that the photoinduced holes drift outward to the ITO layer under the impact of the built-in electric field (E_{in}), which is directed to the ITO layer near the n-Si surface (Figure S2). From the capacitance−voltage profiling (Figure 3), we notice that the SCR in the Si is totally depleted under equilibrium state after modifying the n-Si/ITO interface with a thin layer of TiO_x, and maintained to be deeply depleted with applying the reverse bias. No extra capacitance−voltage response is observed even under a large reverse voltage range, indicating that the amount of the donor-like defects was largely decreased after the introduction of TiO_x interlayer, and then resulting in a highly efficient charge transfer.

The capacitance−voltage profiling of n-Si/ITO and n-Si/TiO_x/ITO Schottky cells were also checked under illumination to detect the influence of interface defects on photoinduced charge transfer. As shown in Figure 5, both the two cells behave

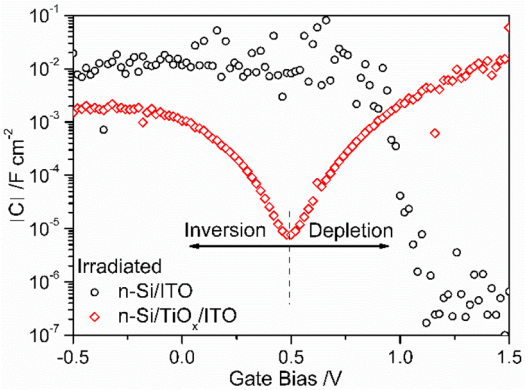

Figure 5. Capacitance−voltage curves recorded for n-Si/ITO and n-Si/TiO_x/ ITO solid cells with 1 kHz AC frequency under illumination.

photoinduced positively charged inversion layer near the n-Si/oxide interface under 0 V applied gate bias, and holes are repelled out to the ITO layer. As for n-Si/TiO_x/ITO cell, a clear light-driven transition from depletion to inversion can be observed in the capacitance−voltage characteristics, which is due to the decreased time constant for minority carrier generation and thinner SCR region under illumination, indicating a lateral transport of charges within the inversion layer.[35,36] It is not the same case with n-Si/ITO cell, in which the amount of charge is sustained and then decreased to a low value under high forward bias. The interfacial states in the n-Si/ITO cell may act as a blocking center, resisting the charge transport over very long distances (Figure S5b).

3.1.3. TiO_x Interlayer and Its Interaction with Interfacial Species. As illustrated above, the introduction of a thin layer of TiO_x can greatly diminish the interfacial donor-like defects and sustain an efficient charge transport, resulting in the enhanced PEC response of the n-Si Schottky photoanodes. Further investigation shows that the electronic transport properties of n-Si/TiO_x/ITO electrodes vary with different TiO_x thickness (Figure 6a). The CV curves shift negatively with initially

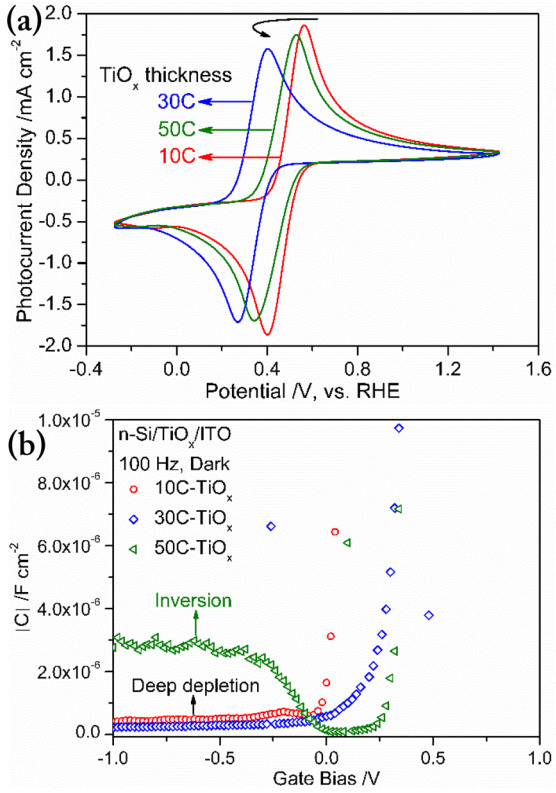

Figure 6. (a) Cyclic voltammetry curves tested in the 5 mM ferri/ferrocyanide solution for n-Si/TiO_x/ITO photoanodes with different TiO_x thickness under 100 mW cm^{-2} of simulated AM1.5 G solar illumination. (b) Capacitance−voltage curves recorded for n-Si/TiO_x/ITO solid cells with different TiO_x thickness under 100 Hz AC frequency in the dark.

increased TiO_x thickness, and then turn to positive potential with further growth of TiO_x. The photoelectrode with 30 cycles (30C) TiO_x presents the lowest oxidation potential for Fe (II), which is in line with the largest E_{FB} and V_{oc} of the n-Si/30C-TiO_x/ITO cell (Figure S6b, c). All of these parameters indicate a highest barrier height and usable photovoltage for n-Si/30C-TiO_x/ITO Schottky junction. From the capacitance−voltage curves and the current−voltage curves (Figures 6b and S6a), it can be seen that the SCR in silicon is totally depleted under equilibrium states in the dark, and the devices all present certain rectification effects irrespective of the TiO_x thickness. If the TiO_x layer is too thin, a more negative gate potential is needed for n-Si/10C-TiO_x/ITO cell to achieve the depletion region, suggesting that the initial introduction of TiO_x species

DOI: 10.1021/jacs.6b07188
J. Am. Chem. Soc. 2016, 138, 13664−13672

fix some positive charges at the interface between n-Si and ITO layer. Further growth of TiO_x can shift the threshold potential positively and the E_{FB} values are almost the same for samples with 30C and 50C TiO_x films. But an excess thickness of TiO_x (50C) will cause an increase of leakage current and weaken the tunneling efficiency, holes will be accumulated near the n-Si surface under reverse bias and appeared as an inversion layer in the capacitance−voltage curves (Figure 6b). This inversion region cannot be detected under high AC frequency, because that the minority carrier generation is unable to follow the high frequency AC signal (Figure S6e).[28] Upon light irradiation, they all present a photoinduced transition from depletion to inversion region, but the n-Si/30C-TiO_x/ITO cell shows the most positive transition potential, which is in line with its largest barrier height (Figure S6d).

Next, intraband electronic states of TiO_x films with different thickness were calculated from the derivative of the Mott−Schottky plots (Figures 7a and S7).[37,38] The TiO_x films

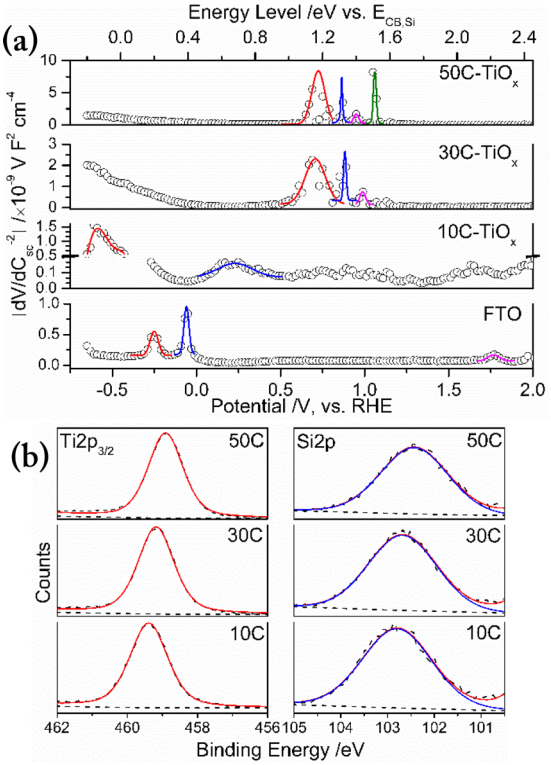

Figure 7. (a) Values taken from the derivative of the nonlinear Mott−Schottky plots in Figure S7. (b) Ti 2p and Si 2p XPS spectra of the n-Si/TiO_x with varied TiO_x thickness.

mentioned in this work were prepared through atom-layered-deposition (ALD) method. Along with being thicken up, these TiO_x films show some different intraband electronic states.[39] The thinnest TiO_x film (10C) seem to behave some discrete energy levels near its conduction band, and the energy levels is shifted to the midgap position for thicker TiO_x film.[40] From the Ti 2p and O 1s XPS spectra (Figures 7b and S8), it is noticed that the binding energy (BE) of the Ti $2p_{3/2}$ peak at 458.9 eV and the O 1s peak at 530.4 eV for 50C-TiO_x indicate the formation of bulk TiO_2.[41] The BE values of the Ti $2p_{3/2}$ shift to the higher energy for samples with thinner TiO_x (10C and 30C). This shift can be attributed to the stronger TiO_x-Si support interaction at low TiO_x coverages, whose BE is higher than those of bulk TiO_2.[42] It suggests quantized properties for 10/30C-TiO_x and near bulk properties for 50C-TiO_x, and all this leads to the different charge transport mechanisms in the n-Si/TiO_x/ITO Schottky devices.

Here, the question is how the TiO_x interacts with the silicon surface and modifies the interfacial electronic states. As aforementioned, the undesired performance of n-Si/ITO could be attributed to the donor-like defect states at the n-Si/ITO interface, locating at about 0.84 eV below the conduction band of n-Si ($E_{CB,Si}$). The midgap energy levels of these TiO_x films were located far below this region except the thinnest one (Figure 7a), which could diminish the undesirable electric activities of the donor-like defects. For bulk SiO_2, the Si 2p has a BE value larger than 103 eV. In this work, the broad Si 2p peaks located at 102−103 eV can be assigned to the reacted Si (Figures 7b and S8), which is present in various oxidation states such as $Si^{2+} \sim Si^{3+}$ (102.2−102.8 eV) derived from interfacial reactions between the surface Si species and the TiO_x overlayer, suggesting the formation of Si−O−Ti interfacial species.[43−45] The charge transfer will take place in the Si−O−Ti species due to the different electronegativities between the Ti and Si atoms, and then the BE of Si 2p varies with the different thickness of TiO_x. These results clearly illustrate the strong interaction between surface Si species and TiO_x overlayer, which induce the optimization of interfacial electronic states.

To sum up, the TiO_x interlayer with a certain thickness is needed to diminish the interfacial donor-like states and to enhance the photovoltaic and PEC performance of n-Si/ITO Schottky junctions. With thinner TiO_x layer, the charges go across the oxide layer through tunneling mechanism. For the samples with thicker TiO_x layer, the charge transfer may be more influenced by the dielectric constants of the oxide layer, results in a decreased photovoltage for n-Si/50C-TiO_x/ITO cell.[14,46,47] For n-Si/TiO_x/ITO photoanode prepared with 30C-TiO_x and 10 nm ITO films, the photo-oxidation potential for $Fe(CN)_6^{4-}$ shows a 600 mV negative shift compared with that obtained with p^{++}-Si/TiO_x/ITO electrode in the dark, which has an intimate relationship with the photovoltage provide by the Schottky junctions (Figure S9b). A longest electron−hole diffusion length can also be expected for n-Si/TiO_x/ITO photoanode with 30C-TiO_x film.

3.2. Role of the Surface Energetics in Enhancing the Barrier Height. According to the Schottky−Mott rule, the barrier height of n-Si Schottky junction is closely related to the work function of surface layer, here it refers to the ITO layer for n-Si/TiO_x/ITO Schottky junction. We introduced a photo-electrodeposition method to coat the ITO surface with a NiOOH layer (Figure S10). The surface potentials of the device with different coating layers were examined by Kelvin probe force microscopy (KPFM) under solution free conditions in air (Figures 8a and S11a).[48] It is found that the n-Si/TiO_x/ITO shows a higher surface potential difference (CPD), and the coating of NiOOH layer only can lead to a drastically decrease of CPD with 320 mV. As the larger work function of the samples corresponds to a more negative value of CPD, the coating of NiOOH on ITO increases the surface work function.

Moreover, the corresponding SPV which reflect the intensity of built-in electric field were acquired with correlated KPFM and transient SPV techniques (Figures 8b and S11b).[37,49] All the structures show the positive SPV signals which indicate the migration of the photogenerated holes to the surface, leading to

DOI: 10.1021/jacs.6b07188
J. Am. Chem. Soc. 2016, 138, 13664−13672

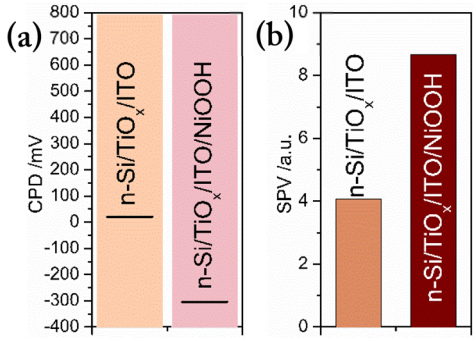

Figure 8. (a) Average contact potential difference of the devices with different coating layers in the dark state and (b) corresponding surface photovoltage.

the increase of surface potential. Decorating the ITO surface with NiOOH layer leads to a 115% increase in SPV signals of the photoanodes. The corresponding SPV signals upon light illumination suggest that the intensity of built-in electric fields for the photogenerated holes separation to the surface of the device follows: Si/TiO$_x$/ITO/NiOOH > Si/TiO$_x$/ITO. Here, we came to the conclusion that the built-in electric field and barrier height of the n-Si/TiO$_x$/ITO Schottky junction can be further enhanced through elevating the work function of the surface layer.

Preceding text has discussed the important role of NiOOH in enhancing the barrier height of photoanode. On conventional views, the NiOOH could act as an OEC, which helps to decrease the activation energy of reactions and reduce charge recombination at the electrode/electrolyte interface. In this system, it is further proved that the surface-modified OECs are bound to interact with the underlying semiconductor, and the surface dipoles or surface states come with these OECs largely influence the energetic alignment of the heterojunction and then the charge separation.[50−52]

3.3. Interfacial Energetics of the n-Si Schottky Photoanode. The SPV results together with the surface potential measurement allow us to draw an energy alignment within and on the surface of the device. First, the barrier height of the unpinned n-Si/TiO$_x$/ITO Schottky junction can be determined from the difference between the electron affinity of the n-type silicon and the work function of the ITO layer. Considering the work function of the ITO layer was usually varies with the preparing condition. So, we estimate the flat band potential of the n-Si/TiO$_x$/ITO Schottky junction from the Mott−Schottky plots (Figure S6c), and the x-intercept of the plots gives a flat band potential of 0.78 V, which is related to the difference in work function between n-Si and ITO. The difference in energy between the Fermi level and the conduction band of n-Si (V_n) was calculated in the calculation section, and V_n is calculated to be 0.17 eV. Considering the measured flat band potential, the n-Si/TiO$_x$/ITO junction presents a barrier height of 0.95 eV. As we know, the silicon has an electron affinity of 4.05 eV. Then, the work function of ITO layer can be estimated from the value of barrier height and the electron affinity of Si, is about 5.0 eV. The calculated work function of the ITO film is close to the highest value reported.[53] It is also proved that the barrier height approaching to the theoretical optimum was realized through the proper interfacial modification of Schottky device.

The band gap of the ALD-TiO$_x$ was about 3.3 eV from the Perego and Wallrapp's results.[40] The redox potential of the NiOOH was 1.22 V (vs RHE) (Figure S10c). All data used in the energy diagram have been elaborated previously. According to the energy alignment shown in Scheme 2, the function of

Scheme 2. Energy Band Diagram of the n-Si/TiO$_x$/ITO/NiOOH Schottky Photoanode under Thermodynamic Equilibrium in the Dark

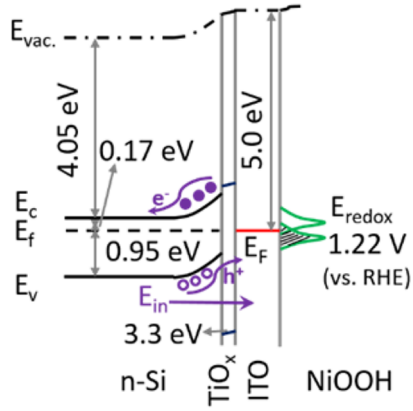

ITO can be elucidated as a collector of holes by constituting the Schottky structure with n-Si and TiO$_x$. The structure is in favor for the photogenerated holes tunneling through the huge barrier.[14,46] Using NiOOH can further increase the surface work function, which leads to the remarkable enhancement of the barrier height and built-in electric field for the migration of photogenerated holes to the electrode surface. Eventually, it results in the enhanced charge separation and a better SPV response, which signifies the role of OECs in charge separation.

3.4. Water Oxidation Performance of the n-Si Photoanodes. HRTEM and EDS mapping were measured to check the structure information on the n-Si/TiO$_x$/ITO/NiOOH photoanode. As shown in Figure 9, uniform and continuous films can be observed for each layer. The EDS mapping clearly depict the composition of each film. TiO$_x$ was prepared through ALD method with 30 growth cycles, it gives a thickness of 2.5−3 nm and presents as an amorphous film. The intrinsic SiO$_x$ was hardly to be distinguished from TiO$_x$ layer, indicating that the intrinsic SiO$_x$ film is very thin and it forms an intimate contact with TiO$_x$. This strong interaction have also been proved between surface Si species and TiO$_x$ overlayer, which induce the optimization of interfacial electronic states (Figure 7). ITO film was crystalline and shows a thickness of 15 nm. NiOOH was fabricated through electro-oxidation deposition method for 2200 s, and it presents a thickness of about 140 nm. The NiOOH film gives a porous morphology, which is commonly observed for layered hydroxide (Figure S15).

Many efforts were made to better understand the properties of these electrodes. Employing 10 nm ITO layer with a thin layer 30C-TiO$_x$, almost 100% light transmittance was realized at 560−880 nm wavelength (Figure S12a). This is favorable for the application of n-Si/TiO$_x$/ITO cells in solar energy conversion. But a poor water oxidation performance was observed for n-Si/TiO$_x$/ITO photoanode in 1 M LiOH (Figure 10a). The charge separation (Φ_{sep}) and injection efficiency (Φ_{inj}) were calculated according to the previous method (Figures 10b and S12b).[20] Even through behaving a poor water oxidation performance, the n-Si/TiO$_x$/ITO photoanode still shows a certain efficiency for charge separation, this is caused by the built-in electric field of the Schottky structure. But the n-

DOI: 10.1021/jacs.6b07188
J. Am. Chem. Soc. 2016, 138, 13664−13672

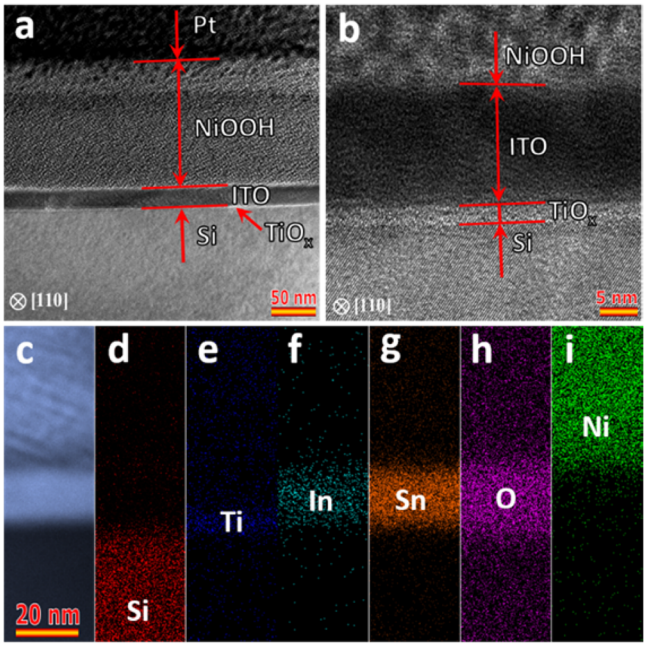

Figure 9. (a, b) Cross-sectional low magnification and High-Resolution TEM images of the n-Si/30C-TiO_x/15 nm-ITO/2200s-NiOOH photoanode (Pt was deposited during sample preparation of TEM). (c) A HAADF-STEM image across the interface. (d–i) Corresponding energy dispersive spectroscopy (EDS) mapping of Si (d), Ti (e), In (f), Sn (g), O (h), and Ni (i).

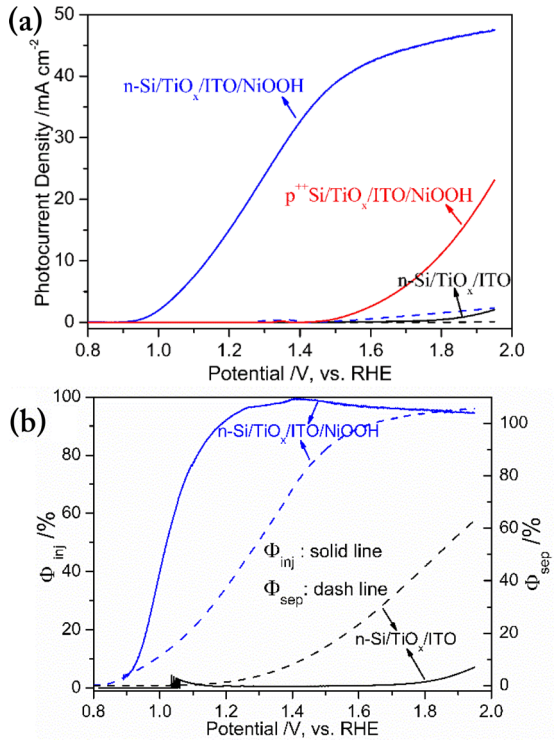

Figure 10. (a) Linear sweep voltammetry curves of n-Si/TiO_x/ITO (black), n-Si/TiO_x/ITO/NiOOH (blue), and p^{++}-Si/TiO_x/ITO/NiOOH (red) photoelectrodes in 1 M LiOH at a 20 mV s^{-1} scan rate. (Solid line, under 100 mW cm^{-2} AM 1.5G irradiation; dashed line, in the dark.) (b) Injection efficiency Φ_{inj} and separation efficiency Φ_{sep} of the n-Si/TiO_x/ITO (black) and n-Si/TiO_x/ITO/NiOOH (blue) photoanodes under 100 mW cm^{-2} AM 1.5G illumination.

Si/TiO_x/ITO photoanode presents a poor charge injection efficiency even under a high applied voltage, proving that its poor water oxidation performance is mainly due to the low efficient charge injection at ITO/electrolyte interface.

Leaving out the promotion role of NiOOH played in enhancing the surface work function of photoanode, the NiOOH is still an OEC with high activity. Once the NiOOH was introduced on the n-Si/TiO_x/ITO, the charge injection was very efficient at a wide voltage range, and extended to above 90% at the potential achieving the saturated current (Figure 10b). The increased charge injection will alleviate the charge recombination at the injecting interfaces, which subsequently extend the carrier lifetime and facilitate the charge separation to some extent.[54] Together with the promotion role of the elevated surface work function to charge separation, the separation of the photogenerated charges occurs at an extremely low potential (~0.8 V, vs RHE), the total charge separation efficiency increases quickly and attains up to 100% at the saturation voltage. This suggests that the impact of OECs on charge separation should be fully comprehended from two aspects mentioned above.

The onset potential is negatively shifted to 0.9 V (vs RHE) and the photocurrent density for water oxidation is also significantly optimized after loading some NiOOH (Figures 10a and S12b). As summarized in Table S4, the onset potential 0.9 V measured in this work is the lowest value of n-Si based photoanodes for water oxidation, accompanied by a high photocurrent density at the equilibrium potential for water oxidation (~18 mA cm^{-2}). This is closely related to the enlarged barrier height of the n-Si/TiO_x/ITO/NiOOH Schottky junction. The PEC performance of the n-Si/TiO_x/ITO/NiOOH photoanode is comparable to that of the np^+ homojunction photoanodes for water oxidation. For n-Si/TiO_x/ITO/NiOOH photoanode, the photocurrent density reaches a saturated value of about 40 mA cm^{-2} at 1.6 V (vs RHE), which is the 91.5% of the theoretical value (43.7 mA cm^{-2}) that crystalline Si can afford, in comparison with p^{++}-Si/TiO_x/ITO/NiOOH electrode in the dark (Figure S10d). This high saturated current density could be attributed to the transparent properties of the TiO_x, ITO and NiOOH layer. This electrode presents almost 100% Faradaic efficiency for water oxidation (Figure S13). The n-Si/TiO_x/ITO device can also be collaborated with many forms of OECs, and they all represent considerable water oxidation activities (Figure S14).

4. CONCLUSIONS

In this article, we clearly demonstrated the important role of the interfacial energetics played in determining the performance of the n-Si Schottky photoelectric devices. The introduction of a thin layer ALD-TiO_x diminishes the donor-like defects at the n-Si/ITO interface, and eliminates the reverse effects of the defects on charge transfer. The barrier height and holes extraction efficiency of the optimized n-Si/TiO_x/ITO junction can be further enhanced through enlarging the work function of the surface layer. All these result in an n-Si/TiO_x/ITO/NiOOH photoanode with an extremely low onset potential of 0.9 V (vs RHE) and a charge separation efficiency approaches to 100% for water oxidation. The strategy developed in this work is not only adapt to the photoanode with Si as the absorber, but also can be applied to the photoanode systems with other semiconductors.

DOI: 10.1021/jacs.6b07188
J. Am. Chem. Soc. 2016, 138, 13664–13672

■ ASSOCIATED CONTENT

Supporting Information

The Supporting Information is available free of charge on the ACS Publications website at DOI: 10.1021/jacs.6b07188.

Materials, experimental details, characterization methods, photoelectrocatalysis measurements, and calculation methods (PDF)

■ AUTHOR INFORMATION

Corresponding Author

*canli@dicp.ac.cn

Notes

The authors declare no competing financial interest.

■ ACKNOWLEDGMENTS

This work was financially supported by 973 National Basic Research Program of the Ministry of Science and Technology (No. 2014CB239403), National Natural Science Foundation of China (No. 21401189 and 21573230), and the 56th Class General Financial Grant from China Postdoctoral Science Foundation (No. 2014M561258). The authors thank Dr. Shuwen Yu and Dr. Wensheng Liang of Dalian Institute of Chemical Physics for useful discussion.

■ REFERENCES

(1) Walter, M. G.; Warren, E. L.; McKone, J. R.; Boettcher, S. W.; Mi, Q.; Santori, E. A.; Lewis, N. S. *Chem. Rev.* **2010**, *110* (11), 6446.

(2) *Solar Cells Materials: Manufacture and Operation*; Markvart, T., Castaner, L., Eds.; Elsevier: Oxford, 2005.

(3) Schottky, W. *Eur. Phys. J. A* **1939**, *113*, 367.

(4) Mott, N. F. *Proc. R. Soc. London, Ser. A* **1939**, *171* (944), 27.

(5) Tung, R. T. *Appl. Phys. Rev.* **2014**, *1*, 011304.

(6) Kim, C. E.; Tak, Y. J.; Butler, K. T.; Walsh, A.; Soon, A. *Phys. Rev. B: Condens. Matter Mater. Phys.* **2015**, *91* (8), 085307.

(7) Pijpers, J. J. H.; Winkler, M. T.; Surendranath, Y.; Buonassisi, T.; Nocera, D. G. *Proc. Natl. Acad. Sci. U. S. A.* **2011**, *108* (25), 10056.

(8) Sun, K.; Saadi, F. H.; Lichterman, M. F.; Hale, W. G.; Wang, H. P.; Zhou, X. H.; Plymale, N. T.; Omelchenko, S. T.; He, J. H.; Papadantonakis, K. M.; Brunschwig, B. S.; Lewis, N. S. *Proc. Natl. Acad. Sci. U. S. A.* **2015**, *112* (12), 3612.

(9) Coridan, R. H.; Arpin, K. A.; Brunschwig, B. S.; Braun, P. V.; Lewis, N. S. *Nano Lett.* **2014**, *14* (5), 2310.

(10) Shaner, M. R.; Fountaine, K. T.; Ardo, S.; Coridan, R. H.; Atwater, H. A.; Lewis, N. S. *Energy Environ. Sci.* **2014**, *7* (2), 779.

(11) Sun, K.; Shen, S.; Cheung, J. S.; Pang, X.; Park, N.; Zhou, J.; Hu, Y.; Sun, Z.; Noh, S. Y.; Riley, C. T.; Yu, P. K.; Jin, S.; Wang, D. *Phys. Chem. Chem. Phys.* **2014**, *16* (10), 4612.

(12) Ashok, S.; FONASH, S. J.; Singh, R.; WILEY, P. *IEEE Electron Device Lett.* **1981**, *2* (7), 184.

(13) Brewer, S. H.; Franzen, S. *J. Phys. Chem. B* **2002**, *106* (50), 12986.

(14) Chen, Y. W.; Prange, J. D.; Duhnen, S.; Park, Y.; Gunji, M.; Chidsey, C. E. D.; McIntyre, P. C. *Nat. Mater.* **2011**, *10* (7), 539.

(15) Schlaf, R.; Murata, H.; Kafafi, Z. H. *J. Electron Spectrosc. Relat. Phenom.* **2001**, *120* (1−3), 149.

(16) Gao, M.; Sheng, W.; Zhuang, Z.; Fang, Q.; Gu, S.; Jiang, J.; Yan, Y. *J. Am. Chem. Soc.* **2014**, *136* (19), 7077.

(17) Zhao, Y.; Jia, X.; Waterhouse, G. I. N.; Wu, L. Z.; Tung, C. H.; O'Hare, D.; Zhang, T. *Adv. Energy Mater.* **2016**, *6* (6), 1501974.

(18) Song, F.; Hu, X. *Nat. Commun.* **2014**, *5*, 4477.

(19) Zhao, Y.; Jia, X.; Chen, G.; Shang, L.; Waterhouse, G. I.; Wu, L. Z.; Tung, C. H.; O'Hare, D.; Zhang, T. *J. Am. Chem. Soc.* **2016**, *138* (20), 6517.

(20) Kim, T. W.; Choi, K. S. *Science* **2014**, *343* (6174), 990.

(21) Wang, L.; Dionigi, F.; Nguyen, N. T.; Kirchgeorg, R.; Gliech, M.; Grigorescu, S.; Strasser, P.; Schmuki, P. *Chem. Mater.* **2015**, *27* (7), 2360.

(22) Hoppe, H. W.; Strehblow, H. H. *Surf. Interface Anal.* **1989**, *14*, 121.

(23) Huang, J. J.; Hwang, W. S.; Weng, Y. C.; Chou, T. C. *Mater. Trans.* **2010**, *51* (12), 2294.

(24) Louie, M. W.; Bell, A. T. *J. Am. Chem. Soc.* **2013**, *135* (33), 12329.

(25) Burke, M. S.; Kast, M. G.; Trotochaud, L.; Smith, A. M.; Boettcher, S. W. *J. Am. Chem. Soc.* **2015**, *137* (10), 3638.

(26) Mills, T. J.; Lin, F.; Boettcher, S. W. *Phys. Rev. Lett.* **2014**, *112* (14), 148304.

(27) Hill, J. C.; Landers, A. T.; Switzer, J. A. *Nat. Mater.* **2015**, *14* (11), 1150.

(28) Scheuermann, A. G.; Kemp, K. W.; Tang, K.; Lu, D. Q.; Satterthwaite, P. F.; Ito, T.; Chidsey, C. E. D.; McIntyre, P. C. *Energy Environ. Sci.* **2016**, *9* (2), 504.

(29) Ray, B.; Baradwaj, A. G.; Boudouris, B. W.; Alam, M. A. *J. Phys. Chem. C* **2014**, *118* (31), 17461.

(30) Roberts, G. I.; Crowell, C. R. *Solid-State Electron.* **1973**, *16* (1), 29.

(31) Roberts, G. I.; Crowell, C. R. *J. Appl. Phys.* **1970**, *41* (4), 1767.

(32) Ragnarsson, L. Å.; Lundgren, P. *J. Appl. Phys.* **2000**, *88* (2), 938.

(33) *Lange's Handbook of Chernistry*, 16th ed.; Speight, J., Ed.; McGraw-Hill Education: New York, 2005.

(34) Faifer, V. N.; Schroder, D. K.; Current, M. I.; Clarysse, T.; Timans, P. J.; Zangerle, T.; Vandervorst, W.; Wong, T. M. H.; Moussa, A.; McCoy, S.; Gelpey, J.; Lerch, W.; Paul, S.; Bolze, D. In *2007 International Conference on Frontiers of Characterization and Metrology*; Seiler, D. G., Diebold, A. C., McDonald, R., Gamer, C. M., Herr, D., Khosla, R. P., Secula, E. M., Eds.; American Institute of Physics: Gaithersburg, MD, 2007; Vol. *931*, p 246.

(35) Esposito, D. V.; Levin, I.; Moffat, T. P.; Talin, A. A. *Nat. Mater.* **2013**, *12* (6), 562.

(36) Lopez, D.; Monsieur, F.; Balestra, F. In *2008 26th International Conference on Microelectronics (MIEL 2008)*; IEEE: Nis, Serbia, 2008; p 583.

(37) Zhu, J.; Fan, F.; Chen, R.; An, H.; Feng, Z.; Li, C. *Angew. Chem., Int. Ed.* **2015**, *54* (31), 9111.

(38) Tomkiewicz, M. *J. Electrochem. Soc.* **1979**, *126* (9), 1505.

(39) Mi, Y.; Weng, Y. *Sci. Rep.* **2015**, *5*, 11482.

(40) Perego, M.; Seguini, G.; Scarel, G.; Fanciulli, M.; Wallrapp, F. *J. Appl. Phys.* **2008**, *103* (4), 043509.

(41) Dementjev, A. P. *J. Vac. Sci. Technol., A* **1994**, *12* (2), 423.

(42) Lassaletta, G.; Caballero, A.; Wu, S.; Gonzalez-Elipe, A. R.; Fernandez, A. *Vacuum* **1994**, *45* (10), 1085.

(43) Cho, Y. S.; Heo, J. S.; Kim, J. C.; Moon, S. H. *Chem. Vap. Deposition* **2006**, *12* (11), 659.

(44) Alfonsetti, R.; De Simone, G.; Lozzi, L.; Passacantando, M.; Picozzi, P.; Santucci, S. *Surf. Interface Anal.* **1994**, *22*, 89.

(45) Sasahara, A.; Pang, C. L.; Tomitori, M. *J. Phys. Chem. C* **2010**, *114* (47), 20189.

(46) Scheuermann, A. G.; Prange, J. D.; Gunji, M.; Chidsey, C. E. D.; McIntyre, P. C. *Energy Environ. Sci.* **2013**, *6* (8), 2487.

(47) Scheuermann, A. G.; Lawrence, J. P.; Kemp, K. W.; Ito, T.; Walsh, A.; Chidsey, C. E.; Hurley, P. K.; McIntyre, P. C. *Nat. Mater.* **2015**, *15* (1), 99.

(48) Melitz, W.; Shen, J.; Kummel, A. C.; Lee, S. *Surf. Sci. Rep.* **2011**, *66* (1), 1.

(49) Kronik, L.; Shapira, Y. *Surf. Sci. Rep.* **1999**, *37* (1−5), 1.

(50) Zhang, Z.; Yates, J. T., Jr. *J. Phys. Chem. Lett.* **2010**, *1* (14), 2185.

(51) MacLeod, B. A.; Steirer, K. X.; Young, J. L.; Koldemir, U.; Sellinger, A.; Turner, J. A.; Deutsch, T. G.; Olson, D. C. *ACS Appl. Mater. Interfaces* **2015**, *7* (21), 11346.

(52) Smith, W. A.; Sharp, I. D.; Strandwitz, N. C.; Bisquert, J. *Energy Environ. Sci.* **2015**, *8* (10), 2851.

(53) Schlaf, R.; Murata, H.; Kafafi, Z. H. *J. Electron Spectrosc. Relat. Phenom.* **2001**, *120*, 149.

DOI: 10.1021/jacs.6b07188
J. Am. Chem. Soc. 2016, 138, 13664−13672

(54) Han, T. H.; Kim, Y. H.; Kim, M. H.; Song, W.; Lee, T. W. *ACS Appl. Mater. Interfaces* **2016**, *8* (9), 6152.

DOI: 10.1021/jacs.6b07188
J. Am. Chem. Soc. 2016, 138, 13664−13672